

# Developing a Coarse-Grained Model for Bacterial Cell Walls: Evaluating Mechanical Properties and Free Energy Barriers

Rakesh Vaiwala, Pradyumn Sharma, Mrinalini Puranik, and K. Ganapathy Ayappa\*

Cite This: *J. Chem. Theory Comput.* 2020, 16, 5369–5384

Read Online

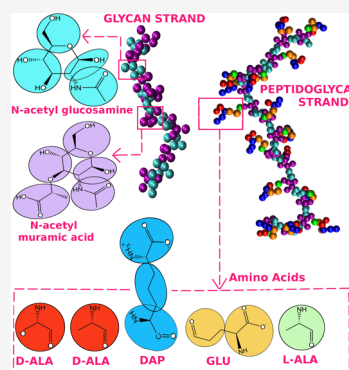
ACCESS |

Metrics & More

Article Recommendations

Supporting Information

**ABSTRACT:** The bacterial cell envelope of Gram-negative bacteria is a complex biological barrier with multiple layers consisting of the inner membrane, periplasm of peptidoglycan, and the outer membrane with lipopolysaccharides (LPS). With rising antimicrobial resistance there is increasing interest in understanding interactions of small molecules with the cell membrane to aid in the development of novel drug molecules. Hence suitable representations of the bacterial membrane are required to carry out meaningful molecular dynamics simulations. Given the complexity of the cell envelope, fully atomistic descriptions of the cell membrane with explicit solvent are computationally prohibitive, allowing limited sampling with small system sizes. However, coarse-grained (CG) models such as MARTINI allow one to study phenomena at physiologically relevant length and time scales. Although MARTINI models for lipids and the LPS are available in literature, a suitable CG model of peptidoglycan is lacking. Using an all-atom model described by Gumbart et al. [*PLoS Comput. Biol.* 2014, 10, e1003475], we develop a CG model of the peptidoglycan network within the MARTINI framework. The model is parametrized to reproduce the end-to-end distance of glycan strands. The structural properties such as the equilibrium angle between adjacent peptides along the strands, area per disaccharide, and cavity size distributions agree well with the atomistic simulation results. Mechanical properties such as the area compressibility and the bending modulus are accurately reproduced. While developing novel antibiotics it is important to assess barrier properties of the peptidoglycan network. We evaluate and compare the free energy of insertion for a thymol molecule using umbrella sampling on both the MARTINI and all-atom peptidoglycan models. The insertion free energy was found to be less than  $k_B T$  for both the MARTINI and all-atom models. Additional restraint free simulations reveal rapid translocation of thymol across peptidoglycan. We expect that the proposed MARTINI model for peptidoglycan will be useful in understanding phenomena associated with bacterial cell walls at larger length and time scales, thereby overcoming the current limitations of all-atom models.



## INTRODUCTION

Bacterial cells are surrounded by cell envelopes with a distinct architecture. In Gram-negative bacteria, cells are protected by an inner phospholipid bilayer membrane, a periplasmic space containing a cell wall made up of peptidoglycan, and an outer membrane consisting of asymmetric leaflets of phospholipids and lipopolysaccharides.<sup>2</sup> In the absence of the outer membrane, the cell wall for Gram-positive bacteria consists of a relatively thick peptidoglycan structure. Peptidoglycan, also known as murein, is the main stress-bearing component of bacterial cells, resisting internal turgor pressure and determining the eventual shape of the cell. A molecular understanding of the bacterial cell membrane and its components play a key role in development of persistence in antimicrobial resistance (AMR) bacterial strains. Several antibiotics directly target various components of the cell membrane; for example colistin targets lipopolysaccharides,<sup>3</sup> vancomycin inhibits synthesis pathways of peptidoglycan,<sup>4</sup> and lysins enzymatically degrade peptidoglycan.<sup>5</sup> In this manuscript our primary focus lies in developing a coarse grained model for peptidoglycan.

In its architecture, peptidoglycan is a mesh-like structure constructed by oligomeric strands of glycans, cross-linked by

stems of peptides (muropeptides). The glycan strands are polymers made up of alternating units of N-acetylglucosamine (NAG) and N-acetylmuramic acid (NAM). A short peptide containing 5 amino acids is attached to the lactyl moiety of each NAM residue.<sup>6</sup> The usual sequence of the amino acids in the penta-peptide is L-alanine (L-ALA), D-isoglutamate (GLU), meso-diamino pimelic acid (DAP), D-alanine (D-ALA), and D-alanine (D-ALA).<sup>7</sup> The molecular structures of these sugar units and the peptide forming amino acids are illustrated in Figure 1A. In general, the periplasm containing peptidoglycan is multilayered,<sup>8</sup> with the exception of *Escherichia coli* which has more than 75% of glycan strands arranged in a monolayer<sup>9</sup> with a thickness of 4 nm.<sup>10</sup> Glycan strands show a broad distribution of lengths, with a mean

Received: May 27, 2020

Published: July 6, 2020



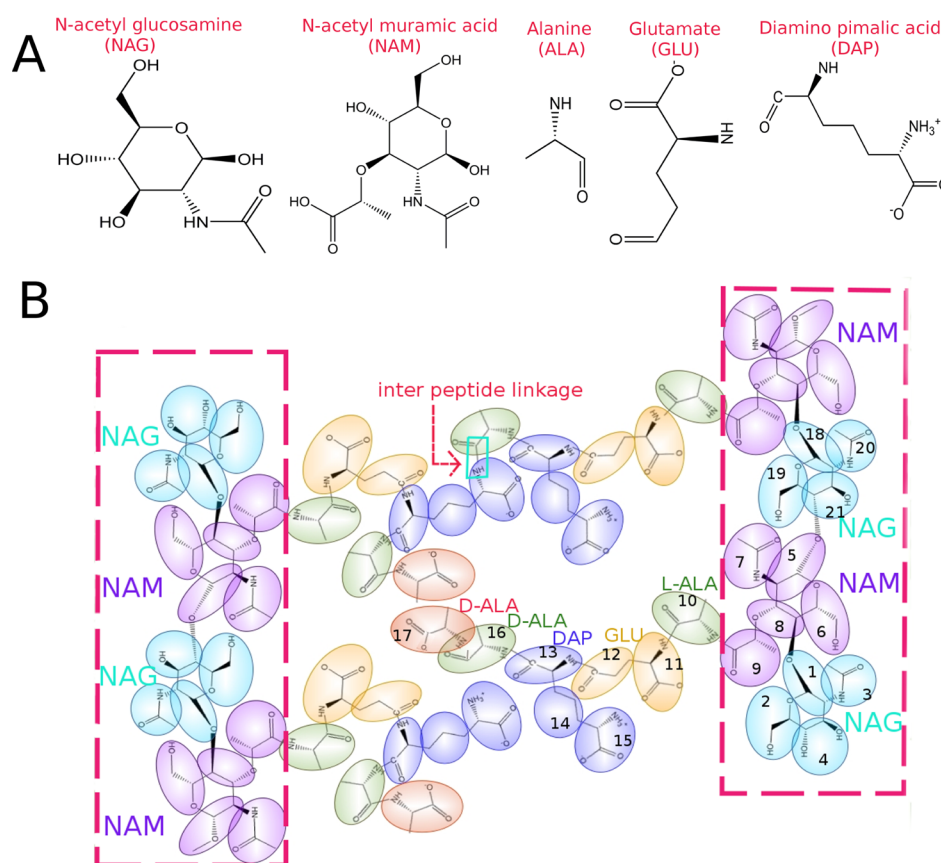


**Figure 1.** (A) Atomic structures of the molecular building blocks in construction of peptidoglycan. (B) Schematic showing an atomic structure of peptidoglycan strands (each 2-mer long) and coarse-grained mapping scheme with tinted MARTINI beads superimposed upon the underlying atomic structure. Coarse graining from the all-atom structure to the MARTINI model results in about 7 fold reduction in the number of atoms. Each mer is represented by 17 beads in the MARTINI force field, and the numeric indicates the bead labels. The glycan strands are shown within the boxes, and the ordering of amino acids from a sugar backbone is L-ALA, GLU, DAP, D-ALA, and D-ALA. As indicated by a small rectangle, a pair of peptides is covalently bonded via inter peptide linkage to form a cross-link between the glycan strands. While linking the peptides, the terminal residue D-ALA in one of the peptides is eliminated.

length ranging from 21 to 40 disaccharides of NAG and NAM residues.<sup>11,12</sup> A single disaccharide (1-mer unit) is of length 1.03 nm.<sup>13</sup>

To understand the organization of the glycan strands relative to the cell surface, two diverse models were proposed based on electron microscopy experiments.<sup>14,15</sup> According to the “circumferential layered” model,<sup>14</sup> glycan strands orient parallel to the cell surface. In contrast, the “scaffold” model assumes that the strands protrude out from the cytoplasmic membrane perpendicular to the cell surface.<sup>15</sup> The relatively thin ( $\leq 4$  nm) *E. coli* cell surface and the orientation of wrinkles in electron tomography data<sup>10</sup> support the circumferential model which has been widely used while developing models for peptidoglycan.<sup>1,16,17</sup> Several models for peptidoglycan ranging from all-atom to supra coarse-grained have been developed in the literature, and we review them next.

Using energy minimization in an all-atom model Leps et al.<sup>18</sup> computed energetically favorable conformations of the glycan backbone and found that the backbone adopts extended structures with each disaccharide spanning 0.98–1.02 nm in length. The lactyl sites in NAM orient away from the murein backbone, and the propagation angle between subsequent sites is found to be 80–100°. Koch<sup>19</sup> extended the conformational analysis for a penta-muropeptide, and a nona-muropeptide in aqueous and cytoplasmic environments. A three-dimensional

structure of the bacterial cell wall was proposed by Meroueh et al.<sup>20</sup> using molecular dynamics simulations on a network formed by 8-mer long peptidoglycan strands. The peptides adopted 3-fold symmetry of orientation along the glycan helices, with a minimum pore diameter of 7 nm in the mesh structure. In an atomistic MD simulation of peptidoglycan Gumbart et al.<sup>1</sup> captured the monolayer thickness, pore size, and anisotropic elasticity in two orthogonal directions of glycans and peptides in general agreement with experimental data, supporting the disordered circumferential model of peptidoglycan. The model exhibits strain stiffening behavior at moderate to high surface tension.<sup>21</sup> In other studies, stable interactions of lysozyme with glycan reveal that O-acetylated glycan is highly distorted, disrupting interactions with lysozyme.<sup>22</sup> An atomistic model of peptidoglycan compatible with a CHARMM36 force field was employed recently by Kim et al.<sup>23</sup> to investigate structural rearrangement of nascent peptidoglycan in the presence of penicillin-binding protein (PBP1b).

In addition to atomistic and coarse grained molecular descriptions for bacterial cell walls, a few models which permit studying deformations of the entire cell wall have been developed. Huang et al.<sup>16</sup> developed a model for peptidoglycan using a network of springs to capture the mechanical response of *Escherichia coli* cells. The model incorporates the forces due

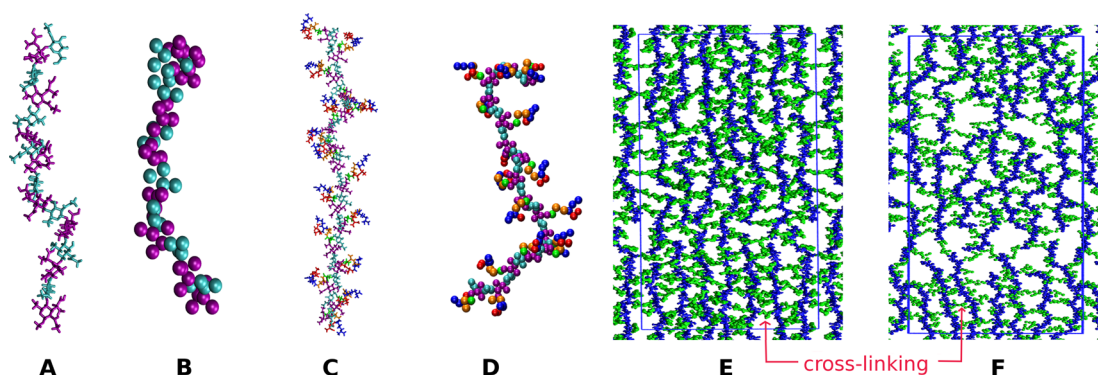


**Figure 2.** Simulated systems: (from left to right) an 8-mer glycan strand in all-atom (A) and MARTINI (B) simulations, a 16-mer peptidoglycan chain in all-atom (C) and MARTINI (D), and a network composed of 21 peptidoglycan strands in all-atom (E) and MARTINI (F) simulations. The color codes for panels A–D refer to NAG (cyan), NAM (purple), L-ALA (green), GLU (orange), DAP (blue), and D-ALA (red), while for the network of glycan strands the sugar backbones are represented by blue color and peptides are shown in green. The rectangular box shows the periodic boundaries in  $x$ – $y$  plane. Solvent and ions are not shown for visual clarity.

to springs, bending, and the osmotic pressure difference at vertices formed by peptides and glycan springs. The mechanical response of cell shape to cell wall damage was predicted. A supra coarse-grained model of the cell wall sacculus was developed by Nguyen et al.<sup>17</sup> to study remodeling of peptidoglycan during biosynthesis and growth of the cell wall. With local coordination of enzymes, the model sacculus prevents local defects caused by new material introduced via transpeptidation and transglycosylation, enabling enzymes to move along the glycan hoops, thereby maintaining cell wall integrity and rod-like shape.

Syma Khalid and co-workers<sup>24–26</sup> have developed several models for the outer membrane of Gram-negative bacteria using united atom as well as MARTINI representations. Using united atom simulations, Samsudin et al.<sup>27</sup> reveal the manner in which the distance between outer membrane porins such as OmpA and peptidoglycan is reduced due to binding of OmpA C-terminus residues and the Braun's lipoprotein with peptidoglycan. Additionally binding of the C-terminus residues was found to assist the dimerization of OmpA in the absence of Braun's lipoprotein. In a more complex model of the membrane by Boags et al.,<sup>28</sup> which included peptidoglycan, the inner membrane with TolR protein and the outer membrane with an OmpA dimer, the authors illustrate the role of noncovalent interactions in positioning the peptidoglycan layer in the presence of the TolR protein.

Simulating a model bacterial cell envelope with atomic details is computationally demanding, especially when time and length scales involved in membrane-associated collective phenomena are order of milliseconds and micrometers, respectively. Under such circumstances, coarse-grained (CG) models of the bacterial cell are ideally suited for large scale molecular simulations, allowing relatively larger systems to be investigated over longer time scales. Therefore, there exists a variety of coarse-grained models for lipids, amino acids, carbohydrates, and nucleic acids. The methodology to devise the coarse-grained model parameters ranges from solvent-free models to more realistic explicit models that include chemical specificity.

MARTINI force fields for coarse-grained simulations were originally developed for lipids and cholesterol.<sup>29</sup> Subsequently the MARTINI force field was extended to carbohydrates,<sup>30</sup> proteins,<sup>31</sup> and nucleotides.<sup>32,33</sup> The bonded parameters for monosaccharides such as glucose and fructose and disacchar-

ides such as sucrose, maltose, and cellobiose are optimized to match the conformations obtained from all-atom (AA) simulations. The CG models of 20 amino acids are systematically parametrized using 2000 proteins from the Protein Data Bank.<sup>31</sup> Following the MARTINI philosophy, López et al.<sup>34</sup> proposed CG models for more than 5 types of glycolipids. The model membranes of glycolipids are tested for their structural properties such as electron density, area per lipid, and the membrane thickness. The MARTINI models are not without drawbacks.<sup>35</sup> For instance, MARTINI sugars are sticky and form aggregates at concentrations below their solubility limits.<sup>36</sup> The protein–protein interactions are unrealistic, giving rise to excessive free energies for protein dimerization.<sup>37</sup> By scaling down the well-depth of Lennard-Jones interactions, exaggerated clustering of proteins and aggregation of sugars can be alleviated.<sup>36,38</sup>

Here we develop a MARTINI model for peptidoglycan by using an atomistic model developed by Gumbart and co-workers.<sup>1</sup> Coarse graining is carried out at various levels of increasing complexity in order to develop a robust MARTINI model for a peptidoglycan chain and a peptidoglycan network. At each level mapping is systematically carried out with the reference all-atom simulations in explicit water. Using a peptidoglycan network consisting of 21 glycan strands which are equivalent to 0.5 million atoms in all-atom simulations, we evaluate the end-to-end distance, stretch modulus, bending modulus, density distributions and voidage in the peptidoglycan networks. Although there are recent studies attempting to understand antimicrobial activity of small molecules with the complex outer membrane of bacteria,<sup>39–41</sup> the interaction of peptidoglycan with molecules has not been reported. To our knowledge, this is the first study to investigate the interactions of a small molecule with peptidoglycan. Potential of mean force computations carried out using MARTINI and all-atom models illustrate a low barrier for translocation through the peptidoglycan layer.

## ■ SIMULATION METHODS

Following the bottom up approach, a MARTINI model of peptidoglycan is devised by mapping the distributions for bonds, angles, and dihedrals on the target distributions, which are derived from the virtual CG-trajectories obtained in all-atom simulations. To develop the CG model in a systematic manner, we have carried out all-atom and MARTINI

Table 1. Summary of Simulation Systems

system	atomistic simulation				MARTINI simulation			
	glycan atoms	TIP3/ions	size (nm)	time (ns)	glycan beads	P4/ions	size (nm)	time ( $\mu$ s)
8-mer glycan	510	32611/0	10 $\times$ 10 $\times$ 10	200	72	35192/0	16 $\times$ 16 $\times$ 16	2
16-mer glycan	1014	261878/0	20 $\times$ 20 $\times$ 20	200	144	276036/0	32 $\times$ 32 $\times$ 32	2
8-mer PG chain	1054	52072/16 K <sup>+</sup>	10 $\times$ 16 $\times$ 10	200	136	35167/16 Na <sup>+</sup>	16 $\times$ 16 $\times$ 16	4
16-mer PG chain	2102	49733/32 K <sup>+</sup>	8 $\times$ 24 $\times$ 8	200	272	275973/32 Na <sup>+</sup>	32 $\times$ 32 $\times$ 32	3
PG network-1	11664	53948/182 K <sup>+</sup>	14 $\times$ 14 $\times$ 5	100	1517	13686/182 Na <sup>+</sup>	14 $\times$ 14 $\times$ 5	0.5
PG network-2	39184	179920/616 K <sup>+</sup>	15 $\times$ 41 $\times$ 9	50	5140	58401/616 Na <sup>+</sup>	15 $\times$ 41 $\times$ 12	0.2

simulations on systems with a single glycan strand in water, a peptidoglycan chain containing peptides in water, and peptidoglycan networks as depicted in Figure 2. All simulations are performed on GROMACS package,<sup>42</sup> version 5.1.5, at 310 K and 1 bar pressure unless stated otherwise. The system size, number of solvent molecules and glycan atoms, and run time details are given in Table 1. For AA simulations we have adopted CHARMM36 force field parameters given in the work of Gumbart et al.<sup>1</sup> Molecular topology files for glycan strands are provided in the Supporting Information (SI), while the topology files for the networks are available upon request.

Referring to Figure 1, a glycan strand comprises alternating units of *N*-acetylglucosamine (NAG) and *N*-acetylmuramic acid (NAM). The glycan strand in peptidoglycan has peptide stems covalently bonded with  $\alpha$ -lactyl groups of the NAM residues. In the network of peptidoglycan, glycan strands are cross-linked via their peptides by bridging a bond between the DAP residue in an acceptor peptide and the penultimate D-ALA residue of a donor peptide, as illustrated in Figure 1B. It is to be noted that during the dimerization of peptides, the terminal D-ALA in the donor peptide is eliminated.

**Atomistic Simulations.** Below we describe all-atom (AA) simulation details for each of the systems given in Table 1. The atom types, mass, partial atomic charges, etc. are specified in the molecular topology files provided in the SI.

**Glycan Strands in Water.** The systems comprised of 8-mer and 16-mer glycan strands embedded in water are simulated in an isothermal–isobaric (NPT) ensemble. A constant temperature of 310 K is maintained using a Nosé–Hoover thermostat with a time constant of 1 ps.<sup>43,44</sup> An isotropic pressure coupling with a coupling constant of 5 ps and compressibility  $4.5 \times 10^5 \text{ bar}^{-1}$  is imposed using the Parrinello–Rahman barostat.<sup>45</sup> Verlet cutoff scheme is chosen to compute the nonbonded interactions (Lennard-Jones 6-12), which are truncated at the cutoff radius of 1.2 nm. The nonbonded van der Waals interactions are shifted with a force-switch function between 1.0 to 1.2 nm to render the forces continuous at the cutoff radius. The long ranged Coulomb interactions are computed using the Particle Mesh Ewald<sup>46</sup> method with a real-space cutoff of 1.2 nm. The periodic boundary condition is used in all three directions. The CHARMM TIP3P water model is employed as a solvent. The positions and velocities of the atoms are updated with a time step size of 2 fs using the leapfrog algorithm.

**Peptidoglycan Chains in Water.** An 8-mer strand of glycan with a short peptide of five amino acids is simulated under the conditions mentioned above. The residues GLU and terminal D-ALA have a unit negative charge, and therefore the system is neutralized by adding potassium ions. A trajectory of 200 ns is generated, and the last 100 ns trajectory is analyzed to obtain the distributions for bonded-interactions. In addition to this,

the simulation is repeated for a 16-mer long peptidoglycan chain to verify the reproducibility of the bonded interactions.

**Networks of Peptidoglycan.** A peptidoglycan network (PG network-1) is constructed by cross-linking 7 glycan strands through the peptides. The strands are initially configured with an interstrand distance of  $\sim 2$  nm over a simulation patch of  $14 \times 14$  nm. Each strand of glycan contains 13 units of disaccharides. In order to determine the extent of cross-linking between the adjacent glycan strands, a trial simulation is performed with a harmonic restraint of  $400 \text{ kJ mol}^{-1} \text{ nm}^{-2}$  on the heavy atoms (carbon and oxygen) in sugar rings, while the peptide residues are kept restraint-free. Based on the frequency of contacts with a cutoff distance of 0.8 nm between the free amino group of DAP residue in acceptor peptides and the carbonyl group of D-ALA in donor peptides, the adjacent glycan strands are cross-linked preferentially with 50% linkages.

In addition, a bigger size network of peptidoglycan (PG network-2) comprising of 21 glycan strands of varying length (on average  $\sim 15$  disaccharides long) is simulated for evaluating structural properties. The glycan strands and the peptides are covalently linked across the periodic boundaries, representing an infinitely large network of peptidoglycan.

**Coarse-Grained Simulations.** The MARTINI constructs equivalent to the AA systems just described above are simulated using GROMACS. The MARTINI bead type, mass, charge and other bonded information are given in molecular topology files in the SI. The system size and duration of simulations are given in Table 1.

**Glycan Strands in MARTINI Framework.** The MARTINI simulations are carried out on systems with glycan strands in standard MARTINI water. The glycan strands are 8-mer and 16-mer long in size. The thermostating of 310 K is achieved through velocity rescaling<sup>47</sup> (*v*-rescale) with a time constant  $\tau_t = 1$  ps, and the pressure of 1 bar is maintained using the barostat of Parrinello–Rahman<sup>45</sup> with a time constant  $\tau_p = 12$  ps and compressibility  $3 \times 10^{-4} \text{ bar}^{-1}$ . The systems are periodic in three dimensions. The van der Waals (LJ) interactions are evaluated using Verlet cutoff scheme with a cutoff distance of 1.1 nm. Equations of motion are integrated using the leapfrog algorithm with a time stepping of 20 fs. The optimized parameters for bonded-interactions, namely bonds, angles and dihedrals, are provided in Tables 2–4. The simulations with the optimized parameters are extended up to 2  $\mu$ s. We have used the MARTINI force field (version 2.2), with a scaled down energy parameter ( $\epsilon$ ) for LJ interactions.<sup>36</sup>

**Peptidoglycan Chains in MARTINI Framework.** An 8-mer long peptidoglycan chain composed of sugars and peptides is modeled using MARTINI beads, and simulated at the conditions mentioned above. Sodium ions (MARTINI v.2.0) are added to neutralize the charges on DAP and terminal D-ALA residues. The long ranged electrostatic interactions are treated using the reaction field method<sup>48</sup> with a screening

Table 2. MARTINI Parameters for Bonds in Glycan Strand<sup>a</sup>

label	beads	bond-length, $r_0$	
		nm	stiffness, $k_b$ kJ mol <sup>-1</sup> nm <sup>-2</sup>
B1	1-2	0.330	constraint
B2	1-3	0.300	8800
B3	1-4	0.309	constraint
B4	2-4	0.350	30000
B5	5-6	0.331	constraint
B6	5-7	0.290	19000
B7	5-8	0.312	constraint
B8	6-8	0.348	21000
B9	8-9	0.299	11050
B10	1-8	0.292	20500
B11	5-21	0.294	20500

<sup>a</sup>Bead labels are according to Figure 1.Table 3. MARTINI Parameters for Angles in Glycan Strand<sup>a</sup>

label <sup>b</sup>	beads	angle, $\theta_0$	
		degree	stiffness, $k_\alpha$ kJ mol <sup>-1</sup>
A1	3-1-2	149	50
A2	3-1-4	82	150
A3	7-5-6	156	160
A4	7-5-8	83	330
A5	9-8-5	133	620
A6	9-8-6	125	150
A7	2-1-8	94	140
A8	3-1-8	111	60
A9	4-1-8	143	114
A10	1-8-6	72	400
A11	1-8-9	90	100
A12	1-8-5	128	480
A13	6-5-21	82	110
A14	7-5-21	131	70
A15	8-5-21	146	240
A16	5-21-19	71	430
A17	5-21-18	134	530

<sup>a</sup>Figure 1 can be referred for bead labels. <sup>b</sup>Restricted bending potential for angles A7–A17.

constant,  $\epsilon_r = 15$ . The optimized parameters for bonds, angles and dihedrals are given in Tables 5–7. The simulation run time is 4  $\mu$ s. In order to verify the robustness of the model parameters, the simulation is repeated with a 16-mer long chain.

**Peptidoglycan Networks in MARTINI Framework.** A CG network of peptidoglycan (PG network-1) is prepared by assembling and cross-linking the glycan strands, 7 in number, through the peptides. With an interstrand spacing of  $\sim 2$  nm, the length of each glycan strand is 13 disaccharides. In order to connect the peptides to form preferentially dimeric linkages, like in AA simulations, a trial MARTINI simulation is carried out with a harmonic restraint of 150 kJ mol<sup>-1</sup> nm<sup>-2</sup> on one of the beads in each sugar ring (e.g., beads 2, 6, 19, etc. in Figure 1). The frequency of contacts between the DAP residue in acceptor peptides and penultimate D-ALA in donor peptides (e.g., beads forming a cross-link in Figure 1) within a cutoff distance of 0.8 nm determines the potential pairs of peptides to be covalently linked. The percentage cross-linking is restricted to  $\sim 50\%$ .

Table 4. MARTINI Parameters for Dihedrals in Glycan Strand<sup>a</sup>

label <sup>b</sup>	beads	angle $\phi_s$ (degree)	stiffness, $k_\phi$ (kJ mol <sup>-1</sup> )	multiplicity, $n$
D1	3-1-2-4	180	16	1
D2	7-5-6-8	180	16	1
D3	7-5-8-9	-120	12	1
D4	5-6-8-9	-60	10	1
D5	2-1-8-5	-	-	-
D6	2-1-8-6	-40	3	2
D7	2-1-8-9	-130	6	2
D8	3-1-8-5			
D9	3-1-8-6			
D10	3-1-8-9			
D11	4-1-8-5	(-20,-20)	(12,6)	(1,2)
D12	4-1-8-6	(0,0)	(14,6)	(1,2)
D13	4-1-8-9			
D14	6-5-21-18	40	3.5	1
D15	6-5-21-19	45	2.5	1
D16	7-5-21-18	-120	3.5	1
D17	7-5-21-19	-120	2.5	1
D18	8-5-21-18	30	20	1
D19	8-5-21-19	30	20	1

<sup>a</sup>Bead labels are according to Figure 1. <sup>b</sup>Dihedrals D5, D8-D10, and D13 do not require constraints.Table 5. MARTINI Parameters for Bonds in Peptidoglycan Strand<sup>a</sup>

label	beads	bond length, $r_0$ (nm)	stiffness, $k_b$ (kJ mol <sup>-1</sup> nm <sup>-2</sup> )
B1	1-2	0.334	constraint
B2	1-3	0.301	10000
B3	1-4	0.305	constraint
B4	2-4	0.350	33000
B5	5-6	0.330	constraint
B6	5-7	0.290	16000
B7	5-8	0.308	constraint
B8	6-8	0.343	44000
B9	8-9	0.300	21000
B10	1-8	0.300	28500
B11	5-21	0.288	32000
B12	9-10	0.349	14800
B13	10-11	0.354	8140
B14	11-12	0.401	28000
B15	12-13	0.315	8230
B16	13-14	0.343	45000
B17	14-15	0.332	44000
B18	13-16	0.331	constraint
B19	16-17	0.357	25700

<sup>a</sup>Bead labels are as per Figure 1.

A larger network of peptidoglycan (PG network-2) having size  $\sim 15 \times 41$  nm is also constructed using 21 CG glycan strands. The network serves as a more realistic cell wall model, as the glycan strands and peptides are covalently bonded across periodic boundaries. This larger simulation patch is employed for free energy calculations as well as for estimating the mechanical properties, namely area compressibility and bending modulus of the peptidoglycan. The surface-tension parameter in GROMACS is employed for anisotropic pressure coupling to set a desired tension in the MARTINI network.

For assessing the free energy barriers for small molecules, the umbrella sampling simulations were carried out for thymol

Table 6. MARTINI Parameters for Angles in Peptidoglycan Strand<sup>a</sup>

label <sup>b</sup>	beads	angle, $\theta_0$	stiffness, $k_a$
		degree	kJ mol <sup>-1</sup>
A1	3-1-2	153	50
A2	3-1-4	83	165
A3	7-5-6	154	280
A4	7-5-8	86	450
A5	9-8-5	121	510
A6	9-8-6	126	290
A7	2-1-8	90	130
A8	3-1-8	118	100
A9	4-1-8	151	170
A10	1-8-6	70	600
A11	1-8-9	93	180
A12	1-8-5	128	555
A13	6-5-21	113	90
A14	7-5-21	99	100
A15	8-5-21	145	250
A16	5-21-19	76	400
A17	5-21-18	135	970
A18	8-9-10	104	80
A19	9-10-11	107	60
A20	10-11-12	92	100
A21	11-12-13	117	80
A22	12-13-16	108	280
A23	13-16-17	102	220
A24	12-13-14	99	80
A25	13-14-15	151	230
A26	16-13-14	98	285

<sup>a</sup>Bead labels are in accordance with Figure 1. <sup>b</sup>Restricted bending potential for angles A9–A26.

insertion though a monolayer of peptidoglycan. Thymol was parametrized using CGenFF<sup>49</sup> to generate its AA force fields, while an automated parametrization scheme introduced by Bereau and Kremer<sup>50</sup> was used for coarse-graining of thymol. It should be noted that the van der Waals interactions between the peptidoglycan and thymol beads in MARTINI simulations are scaled according to eq 1 using the parameter  $\alpha = 0.7$ , which was used to scale the interaction between the peptidoglycan beads. The interactions of thymol and peptidoglycan with water and ions are unscaled. The CG mapping scheme and the MARTINI bead types for thymol (Figure S1) as well as the histograms for umbrella sampling biasing potential (Figures S2–S4) are given in the SI.

Unlike the PG network-2, the smaller patch of peptidoglycan (PG network-1) is tethered, with the oxygen atoms in sugar backbones in AA model harmonically restrained by a force constant of 500 kJ mol<sup>-1</sup> nm<sup>-2</sup>, while a weak restraint is imposed on the CG beads (2, 6, 19, etc. in Figure 1) containing the oxygen in sugar rings in MARTINI simulations to keep the peptidoglycan sheet more or less planar. The umbrella sampling simulations are performed on a reaction coordinate, which is the distance between the center of mass of the peptidoglycan sheet and the center of mass of thymol along the z-direction- normal to the sheet of peptidoglycan. Steered molecular dynamics simulations are employed to generate initial configurations for the umbrella sampling simulations,<sup>51</sup> and the sampling windows are created at a spacing of 0.1 nm. The thymol molecule is restrained using a harmonic potential with a force constant of 1000 kJ mol<sup>-1</sup> nm<sup>-2</sup>. Each umbrella

Table 7. MARTINI Parameters for Dihedrals in Peptidoglycan Strand<sup>a</sup>

label <sup>b</sup>	beads	angle, $\phi_s$	stiffness, $k_\phi$	multiplicity, $n$
		(degree)	(kJ mol <sup>-1</sup> )	
D1	3-1-2-4	180	10	1
D2	7-5-6-8	180	10	1
D3	7-5-8-9	(180,0)	(7,3)	(1,2)
D4	5-6-8-9	(0,0)	(5,5)	(1,2)
D5	2-1-8-5	(0,0)	(3.5,3)	(1,2)
D6	2-1-8-6	(0,0)	(3.5,3)	(1,2)
D7	2-1-8-9			
D8	3-1-8-5			
D9	3-1-8-6			
D10	3-1-8-9	(0,0)	(8,2)	(1,2)
D11	4-1-8-5			
D12	4-1-8-6	(0,0)	(7,3)	(1,2)
D13	4-1-8-9	(180,180)	(2,3)	(2,3)
D14	6-5-21-18	(180,0)	(6,4)	(1,2)
D15	6-5-21-19			
D16	7-5-21-18			
D17	7-5-21-19			
D18	8-5-21-18	(0,0)	(8,2)	(1,2)
D19	8-5-21-19	(0,0)	(7,3)	(1,2)
D20	8-9-10-11	60	3	2
D21	9-10-11-12	140	3	2
D22	10-11-12-13	(180,0)	(5,5)	(1,2)
D23	11-12-13-16	180	3.5	1
D24	12-13-16-17	(180,0)	(7,5)	(1,2)
D25	11-12-13-14	(180,0)	(5,5)	(1,2)
D26	12-13-14-15	0	5	1
D27	16-13-14-15	(180,0)	(5.2,3.8)	(1,2)
D28	17-16-13-14	180	6	1

<sup>a</sup>Figure 1 can be referred for bead labels. <sup>b</sup>Dihedrals D7–D9, D11, and D15–D17 do not require constraints.

window is simulated for 150 and 500 ns in AA and MARTINI simulations, respectively. The free energy profile is computed by using the weighted histogram analysis method (WHAM),<sup>52</sup> implemented in GROMACS.

**Model Parameters.** As mentioned earlier, the MARTINI force field (version 2.2) is adopted for nonbonded interactions. The original MARTINI parameters, namely energy  $\epsilon$  and size  $\sigma$ , lead to an aggregation of CG beads for polysaccharides in MARTINI simulations.<sup>36</sup> Increasing the repulsion between CG beads by reducing the energy parameter  $\epsilon$  is found to remedy the issue of bead aggregation. In order to circumvent the aggregation of peptidoglycan chains observed in our MARTINI simulations (Figure S5 in the SI), we uniformly increased the bead–bead repulsion by scaling down  $\epsilon$  with a parameter ( $\alpha$ ) using<sup>36</sup>

$$\epsilon_{ij,\text{scaled}} = 2 + \alpha(\epsilon_{ij,\text{original}} - 2) \quad (1)$$

We varied  $\alpha$  in the range 0.9 to 0.7, and found that the scaling factor  $\alpha = 0.7$  was sufficient to avoid bead aggregation. With  $\alpha = 0.7$  the scaled parameters,  $\epsilon_{ij}$ , are only slightly reduced to a range of 2.0–4.52 kJ/mol from the original MARTINI range 2.0–5.6 kJ/mol. Further with this scaling, the chain end-to-end distance agreed well with the end-to-end distance obtained in all-atom simulations (Table 8). Additionally at this level of scaling, several other key structural and mechanical properties were accurately captured. By increasing the bead–bead repulsion in the MARTINI force field, we have

Table 8. Summary on Properties of Peptidoglycan

property	MARTINI simulation	AA (this work)	literature
end-to-end distance	3.8 nm (8-mer) 7.5 nm (16-mer)	4.1 (8-mer) 8.1 (16-mer)	
peptides orientation	$\sim 90^\circ$	$\sim 90^\circ$	80–100 <sup>o(18)</sup> , 75–105 <sup>o(19)</sup>
thickness	4–4.5 nm	4–4.5 nm	4 nm <sup>(10)</sup> , 3.4–3.9 nm <sup>(1)</sup>
area per disaccharide	2 nm <sup>2</sup>	2 nm <sup>2</sup>	2.5 nm <sup>2(55)</sup> , 2.6–3.1 nm <sup>2(1)</sup>
area compressibility	20–100 mN/m		29–500 mN/m <sup>(21)</sup>
bending modulus	$\sim 1 k_B T$	$\sim 1 k_B T$	
insertion free energy for thymol	$\sim -1$ kJ/mol	$\sim -1$ kJ/mol	

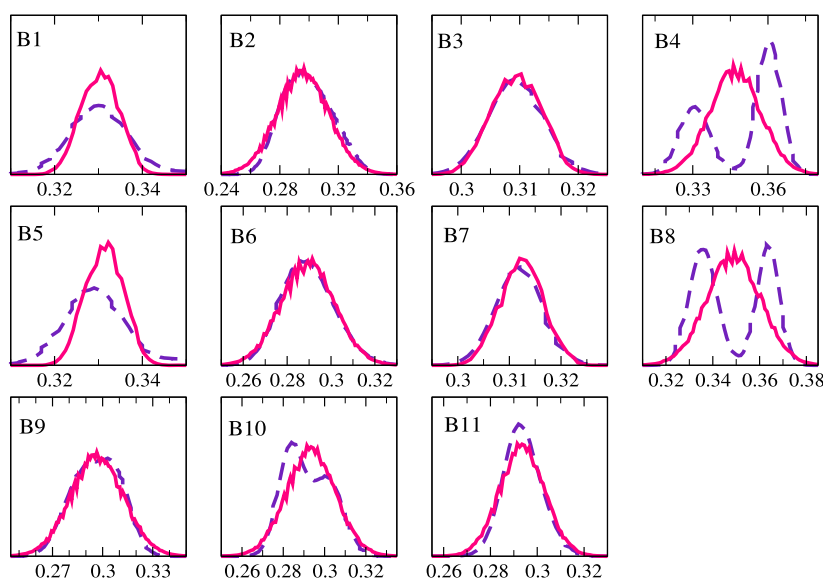


**Figure 3.** Mapping of bond distributions in MARTINI simulations with AA target distributions for an 8-mer glycan strand. Symbols represent AA (—) and MARTINI (---) distributions. The bond lengths are in nm. Table 2 can be referred for bond labels and their corresponding bond parameters.

introduced new bead types, which are distinguished from original MARTINI beads using the letter R. For example, a bead P1 in the original MARTINI force field is now recognized as RP1 with the scaled values of  $\epsilon$ . The interactions of R beads with water (P4) and sodium ions (Q<sub>d</sub>) are unscaled.

The bonded interactions, namely bond-stretching (two body) and angle-bending (three body), are modeled using harmonic springs and cosine potentials, respectively

$$u_{ij}^B = \frac{1}{2} k_b (r_{ij} - r_0)^2 \quad (2a)$$

$$u_{ijk}^A = \frac{1}{2} k_a (\cos(\theta_{ijk}) - \cos(\theta_0))^2 \quad (2b)$$

where  $k_b$  and  $k_a$  represent the bond and angle-bending stiffness constants, while the equilibrium bond lengths and angles are denoted by  $r_0$  and  $\theta_0$ , respectively. In order to avoid numerical instability arising from torsion angle calculations, some of the angles are maintained at their equilibrium values using the restricted bending potential<sup>53</sup>

$$u_{ijk}^A = \frac{1}{2} k_a (\cos(\theta_{ijk}) - \cos(\theta_0))^2 / \sin^2 \theta_{ijk} \quad (3)$$

The torsional angle among quadruple of beads  $i-j-k-l$  is controlled using the cosine function

$$u_{ijkl}^D = k_\phi (1 + \cos(n\phi - \phi_0)) \quad (4)$$

with  $\phi$  being the torsion angle between the planes formed by the triplets  $i-j-k$  and  $j-k-l$ . The stiffness  $k_\phi$ , multiplicity  $n$  and dihedral angle  $\phi_0$  are the model parameters.<sup>54</sup>

The optimized parameters for bonded interactions within the glycan strands are given in Table 2 for bonds, in Table 3 for angles, and in Table 4 for dihedrals. For the peptidoglycan chains, optimized parameters are tabulated in Tables 5–7. When two glycan strands are cross-linked via their peptides, there are additional bonded interactions involving a bond that bridges the peptides and the angles surrounding this bond. The equilibrium bond length at cross-links is 0.35 nm, maintained with a harmonic potential of strength 1100 kJ mol<sup>-1</sup> nm<sup>-2</sup>.

## RESULTS AND DISCUSSION

In this section we explain the procedure for optimizing model parameters, the mapping scheme, selection of MARTINI bead types and validation of the CG models.

**Model Development.** The model parameters for bonded interactions, namely the bond-stiffness  $k_b$ , equilibrium bond length  $r_0$ , angle-bending stiffness  $k_a$ , equilibrium angle  $\theta_0$ , and dihedral parameters, namely  $k_\phi$ ,  $\phi_0$ , and multiplicity  $n$ , are optimized by mapping the bond, angle, and dihedral distributions from MARTINI simulations with the corresponding reference distributions obtained in atomistic simulations. Toward this end, virtual CG trajectories are derived from AA trajectories from the center of mass of groups of atoms forming the CG beads. Figure 1 shows a mapping scheme employed

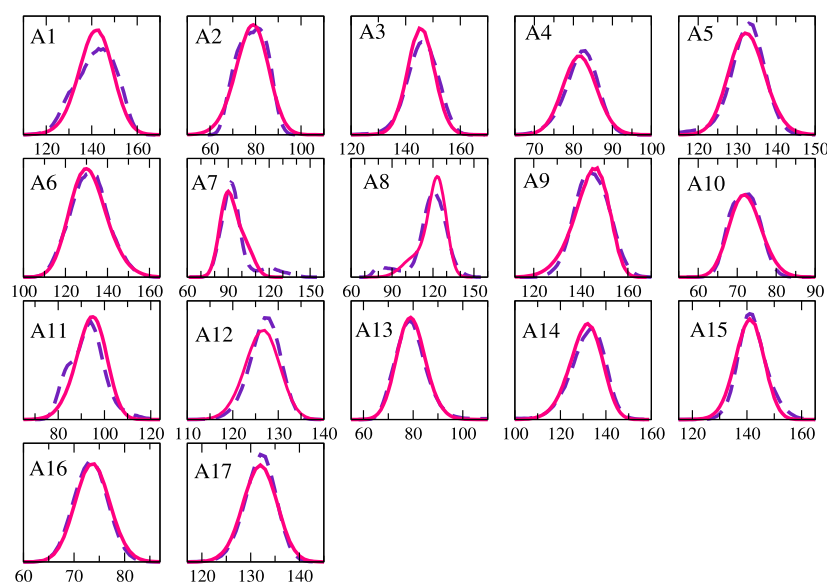


**Figure 4.** Mapping of angle distributions in MARTINI simulations with corresponding AA target distributions for an 8-mer glycan strand. Symbols represent AA (—) and MARTINI (---) distributions. The angles are specified in degrees. The labels and angle parameters are mentioned in Table 3.

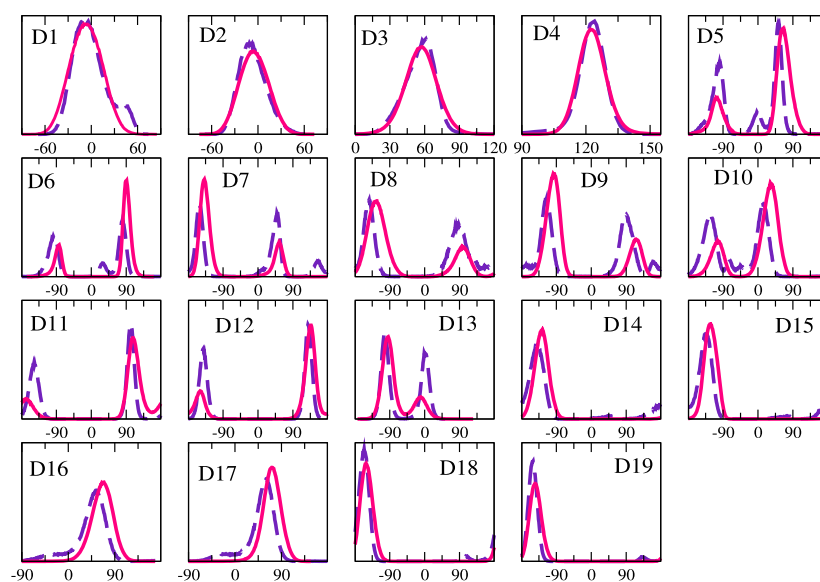


**Figure 5.** Mapping of torsional angle distributions for MARTINI simulations with corresponding AA target distributions for an 8-mer glycan strand. Symbols represent AA (—) and MARTINI (---) distributions. The angles are specified in degrees. The labels are in accordance with Table 4.

during the coarse-graining of peptidoglycan. The coarse-grained beads are assigned appropriate MARTINI bead types based on the functionality (polarity and hydrogen bonding capability) of the underlying atoms within the beads. The particle type “S” is ascribed to smaller size beads in the ring structures of sugar units to mimic a relatively smaller (3:1 or 2:1) mapping compared to the regular 4:1 mapping scheme of MARTINI. Within the MARTINI framework, the polar groups of atoms are labeled with “P” type, while the bead type “N” is used for groups which are partly polar and partly apolar. The charged beads are denoted by “Q”. The apolar beads in peptides are regarded as “AC” for their intrapeptide interactions with “Q” type particles of the peptides.

To begin an iterative process of MARTINI parametrization, the centers of histograms for bonds and angles from AA

simulations of an 8-mer glycan strand are used as an initial set of equilibrium bond lengths and angles in MARTINI simulations. These values are updated after every 500 ns of MARTINI simulation according to

$$X_{\text{new}} = X_{\text{old}} + (X^{\text{AA}} - X^{\text{CG}}) \quad (5)$$

Here  $X$  is the equilibrium bond length (angle) for bond (angle) distributions, while  $X^{\text{AA}}$  and  $X^{\text{CG}}$  are centered at the corresponding distributions in AA and MARTINI simulations, respectively. The strengths of bond-stretching ( $k_b$ ) and angle-bending ( $k_a$ ) are updated according to the heights of the distributions, which are  $Y^{\text{AA}}$  in AA and  $Y^{\text{CG}}$  in the MARTINI simulations, using

$$k_{\text{new}} = k_{\text{old}}(Y^{\text{AA}}/Y^{\text{CG}}) \quad (6)$$

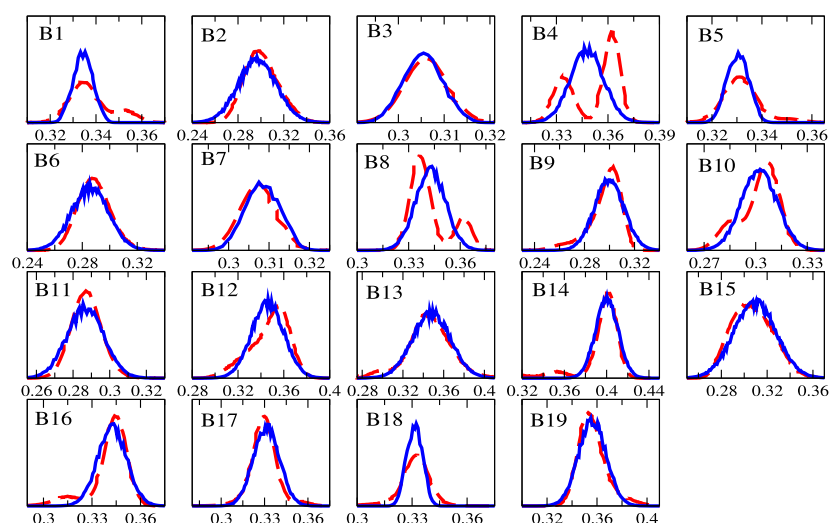


**Figure 6.** Mapping of bond length distributions for MARTINI simulations with corresponding AA target distributions for an 8-mer peptidoglycan strand. Symbol (---) indicates AA distributions, while solid lines (—) represent MARTINI distributions. The bond lengths are in nm. The labels are in accordance with Table 5.

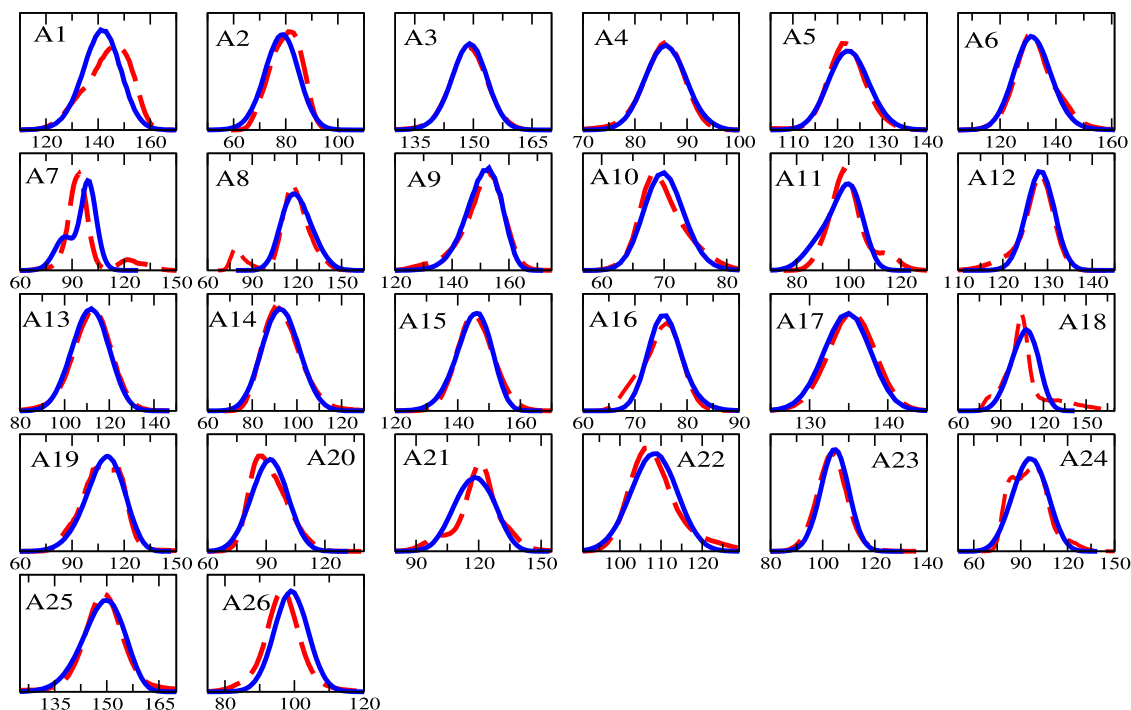


**Figure 7.** Mapping the angle distributions from MARTINI simulations with reference AA distributions for an 8-mer peptidoglycan strand. Symbols represent AA (---) and MARTINI (—) distributions. The angles are specified in degrees. The labels and angle parameters are mentioned in Table 6.

The stiffness constant  $k$  represents  $k_b$  for the bond distributions and  $k_a$  for the angle distributions. The iterative procedure terminates when the bond length in MARTINI simulation converges to its AA counterpart within a tolerance of 0.01 nm and the peak of the distribution lies within 1%. Similarly, the angles are said to be converged when the deviation from their AA target is within  $2^\circ$  and the peak differences are within 1%. The procedure took 3 iterative CG simulations to converge bonds and angles before the dihedrals were set in, and with 8 additional CG simulations the bonded distributions, including 28 dihedrals, were converged. For the bonds showing multimodal distributions, for instance the

bonds labeled by B4 and B8 in Figure 3, we have parametrized the stiffness constant to realize wider CG distributions spanning the multiple peaks observed in the AA distributions. The heights of CG distributions are kept within 2% of the average in the peaks of bimodal distributions. The dihedral parameters, namely the stiffness constant  $k_\phi$ , angle  $\phi_s$  and multiplicity  $n$ , are estimated by considering the number and locations of the peaks in the AA target distributions for the dihedrals. The procedure for parametrization is illustrated in an algorithmic form in Figure S6 of the SI.

**Modeling of Glycan Strand.** The distributions for bonds, angles and dihedrals are computed from a 2  $\mu$ s long trajectory

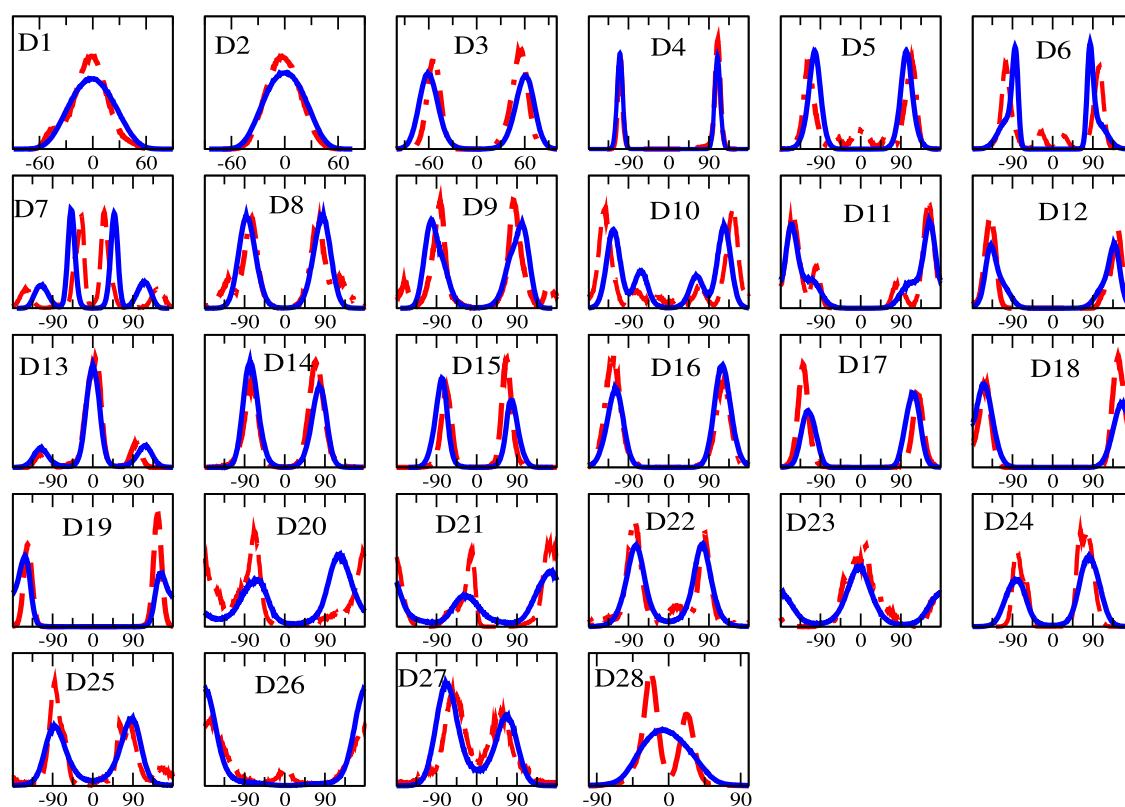


**Figure 8.** Mapping of torsional angle distributions from MARTINI simulations with reference AA distributions for an 8-mer peptidoglycan chain. Symbols represent AA (—) and MARTINI (—) distributions. The angles are specified in degrees. Table 7 can be referred for labels and dihedral parameters.

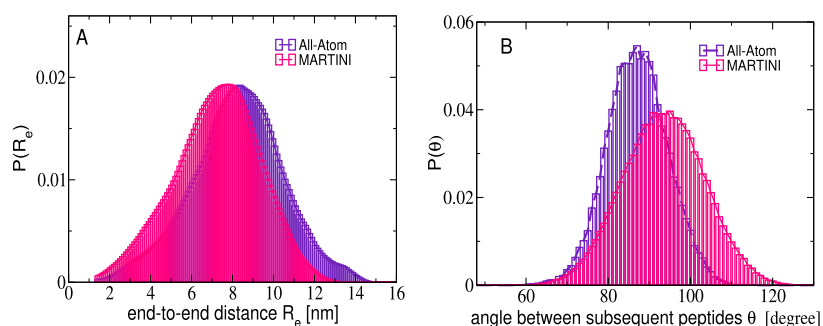


**Figure 9.** (A) Probability distributions of end-to-end distance  $R_e$  for the 16-mer glycan strand in AA (violet) and MARTINI simulations (pink). (B) Probability distributions for the native angle between subsequent peptides along the peptidoglycan chain of 16-mer in AA (violet) and MARTINI simulations (pink).

in a MARTINI simulation of the glycan chain comprising of 8 disaccharides. The last 1  $\mu$ s trajectory is used for averaging. Figure 3 shows an excellent agreement of the bond distributions of the MARTINI simulation with the AA reference distributions. The bond lengths are in the range of 0.29–0.35 nm. The bonds with stiffness constant 50000  $\text{kJ mol}^{-1} \text{nm}^2$  and above are replaced by constraints. The distributions for angles in Figure 4 are also in consonance with their AA counterparts. The mean angles have values over a range of 70–160°. The dihedral distributions that have a single or prominent peak in AA simulations are very well captured by the MARTINI parameters for dihedrals as evidenced in Figure 5. Since the coarse-graining does not retain asymmetrical distributions of atoms that form CG clusters, mapping of dihedrals that have multiple peaks is not always captured. However, for the glycan strands in question,

multimodal peaks are also mapped out satisfactorily, as apparent in Figure 5. The dihedrals having bimodal peaks exhibit two conformers, and such dihedrals are nearly 50% in number. To test the robustness of the MARTINI parameters, we have simulated a 16-mer long glycan strand using the same model parameters obtained for the 8-mer strand. The bonded distributions for the 16-mer strand are given in SI (Figures S7–S9), and their comparison with AA data confirms the validity of the optimized parameters.

**Modeling of Peptidoglycan.** An oligomeric strand having 8 repeating units of disaccharides, with a penta-muropeptide attached to each NAM residue, is simulated using both AA force fields and a MARTINI model. A long trajectory of 2  $\mu$ s in MARTINI simulation is analyzed for the bonded distributions. Figures 6–8 compare the histograms for bonds, angles and dihedrals, respectively, obtained in MARTINI simulations with

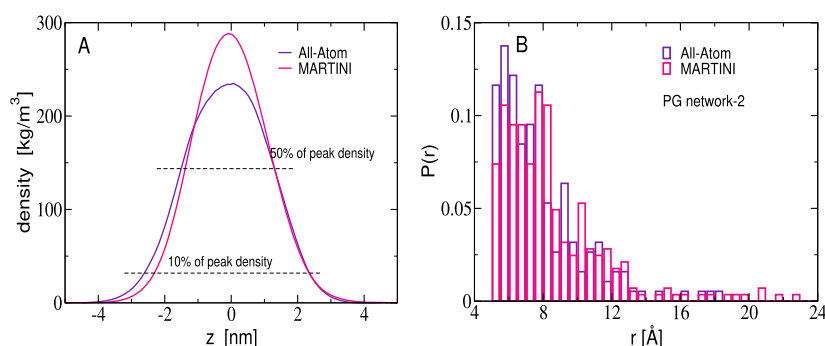


**Figure 10.** (A) Mass density distribution of peptidoglycan in direction ( $z$ ) normal to the plane of the peptidoglycan network containing 21 strands. The symbols are AA model (violet) and MARTINI model (pink). The dash lines at 10% as well as 50% of the peak density serve to estimate the thickness of the peptidoglycan layer. (B) Comparison of cavity size distributions,  $P(r)$ , for CG and AA peptidoglycan networks, which are comprised of 21 glycan strands. The histograms are generated with a bin size of 0.5 Å for cavities of size  $r \geq 0.5$  nm.

those obtained using AA simulations. The matching of the profiles for bonds and angles is excellent. Most of the dihedrals are very well mapped onto their corresponding AA target distributions. The bonded parameters given in Tables 5–7 reproduce the bonded distributions for larger lengths of the peptidoglycan chains, as evidenced in the bonded distributions for a 16-mer peptidoglycan strand in SI (Figures S10–S12).

**Model Validation.** The structural and mechanical properties of the model bacterial cell wall predicted by the proposed MARTINI model are discussed below.

**Glycan Chain End-to-End Distance.** Figure 9A compares the histograms of end-to-end distance ( $R_e$ ) for the 16-mer glycan strand simulated using MARTINI and AA models. The overlap between the histograms is significantly high. The end-to-end distance for the 16-mer CG glycan strand is  $7.5 \pm 0.004$  nm, and this is in good agreement with the end-to-end distance obtained from AA simulation of the 16-mer chain.

**Native Periodicity of Peptides.** NMR spectroscopy study<sup>20</sup> suggests that the successive peptides along a glycan strand are spaced  $\sim 120^\circ$  apart, indicating a 3-fold periodicity in the peptide orientation. However, the computer simulations by Leps et al.<sup>18</sup> revealed that in energetically favorable conformations the consecutive peptides orient with a spacing of  $80$ – $100^\circ$ , and this is further supported by other in-silico investigation reports.<sup>1,19</sup> With a 4-fold symmetry of  $90^\circ$  between the subsequent muropeptides along the glycan strand, half of the peptides would lie in the plane of glycan strands, while the remaining half would protrude out in a direction perpendicular to the plane of glycan strands. Consequently, only 50% of the peptides are accessible to form covalent bonds to cross-links with neighboring glycan strands, supporting experimental evidence of 40–50% cross-linking.<sup>11</sup> Figure 9B depicts an equilibrium angle between consecutive peptides along the sugar chain for the AA and MARTINI models. The propagation angle is found to be  $93.9 \pm 0.02^\circ$  for MARTINI and  $87.5 \pm 0.03^\circ$  for the AA model. The distribution for the angle between consecutive peptides is broader for the MARTINI simulations due to soft coarse-grained beads. The observation of a 4-fold symmetry in orientation of muropeptides is consistent with the literature.<sup>1,18,19</sup>

**Density Distribution.** Figure 10A indicates the mass density of the peptidoglycan normal to the plane of the peptidoglycan network composed of 21 glycan strands. The density profile obtained from the MARTINI model is in good agreement with the AA model of peptidoglycan. Since the total mass of peptidoglycan is conserved between AA and MARTINI

models, a small difference in peak density values is attributed to the differences in their equilibrium lateral areas, which differ by less than 5% relative to the lateral area in the AA simulation. With a criterion of 50% of the peak density, the thickness of the peptidoglycan monolayer is  $\sim 2.5$ – $3.0$  nm. However, the thickness  $\sim 4$ – $4.5$  nm with the 10% criterion of the peak density agrees well with other simulation literature<sup>1</sup> as well as experimental tomograms.<sup>10</sup>

**Voidage in PG Networks.** In order to assess if the MARTINI model was able to capture the cavity size distribution within peptidoglycan we carried out a cavity size analysis<sup>1</sup> using two-dimensional grids. Spheres were inscribed with centers on a fine  $0.1 \times 0.1$  nm grid, and grown until they made contacts with atoms of glycans or cross-linked peptides. A coarser  $1.4 \times 1.4$  nm grid was then laid over the fine grid, and a sphere with a maximum radius was determined from spheres corresponding to the finer grid, which are contained within each cell of the coarser grid. These space-filling spheres embedded in the voids are shown in Figure S13 of the SI. The histograms depicted in Figure 10B (and Figure S14 in the SI) were generated using a lower threshold of 0.5 nm for the minimum cavity size. The agreement between the cavity size distributions obtained from the above procedure of embedded spheres for the CG and AA networks is excellent. The shape of distributions are similar and we observe a small increase toward larger cavities in the tail of the distributions of the MARTINI model.

**Area Per Disaccharides.** The mean area per disaccharide from MARTINI simulations at ambient temperature and pressure is  $\sim 2$  nm<sup>2</sup>, which is consistent with the range 2.6–3.1 nm<sup>2</sup> reported in other atomistic simulations.<sup>1</sup> An experimental mean area per disaccharide was estimated to be  $\sim 2.5$  nm<sup>2</sup> using the number of DAP residues and the surface area of an *Escherichia coli*.<sup>55</sup> This further substantiates the coarse-grained model of peptidoglycan. The area per disaccharide increases with tension in the membrane, as delineated in the next section.

**Area Stretch Modulus.** The monolayer of peptidoglycan comprised of 21 glycan strands (Figure 2F, PG network-2) is subjected to lateral stresses, and its response in areal expansion is monitored. The surface tension is maintained at a desired value, while the pressure ( $P_{zz}$ ) normal to the glycan network is set to 1.0 bar. The surface tension value is varied in a range 0–50 mN/m. The surface tension ( $\gamma$ ) is calculated from the lateral ( $P_{xx}$  and  $P_{yy}$ ) and normal ( $P_{zz}$ ) components of pressure tensor using<sup>56</sup>

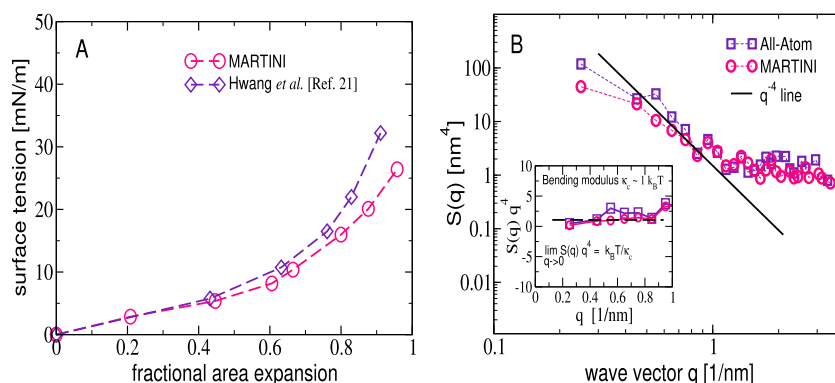


**Figure 11.** (A) Response in area expansion with tension in the MARTINI network of peptidoglycan (PG network-2), and the data represented by  $\diamond$  are extracted from a graph from Hwang et al.<sup>21</sup> (B) Structure factor for height fluctuations in AA ( $\square$ ) and MARTINI ( $\circ$ ) representations of PG network-2, and the  $q^{-4}$  line is a guide to the eye. The inset shows  $S(q)$  data scaled with  $q^4$ , and a horizontal dash line indicating the limiting value  $k_B T / \kappa_c$ .

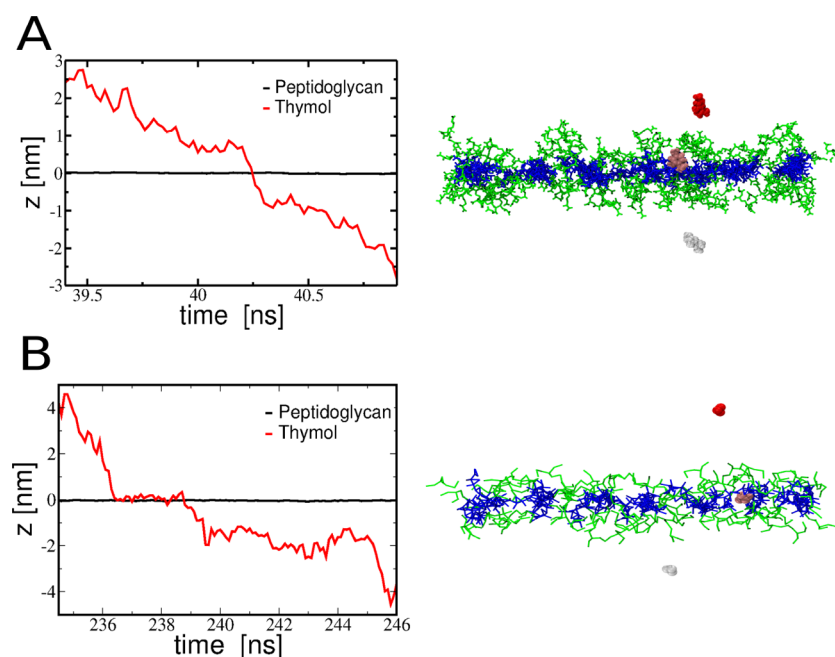


**Figure 12.** Simulation trajectories and snapshots showing a translocation event in restraint-free AA (A) and MARTINI (B) simulations. The center of mass of peptidoglycan (black) is located on a plane at  $z = 0$ , and the center of mass of thymol (red) evolves during the translocation of the molecule. The thymol molecule in the snapshots depicts three instances: before translocation (red), in the membrane (pink), and after translocation (white). Water is not shown for clarity.

$$\gamma = \frac{1}{2} \int_0^{L_z} dz \left( P_{zz} - \frac{P_{xx} + P_{yy}}{2} \right) \quad (7)$$

The simulation box length in the  $z$ -direction is  $L_z$ . Figure 11A shows the variation of the surface tension with the fractional change in lateral area in the plane of peptidoglycan. The lateral area increases with applied tension (Figure S15 in the SI). The area compressibility ( $K_a$ ) of the network is evaluated using

$$K_a = A_0 \frac{\partial \gamma}{\partial A} \Big|_T \quad (8)$$

where  $A_0$  is the equilibrium area at vanishingly zero tension. The area compressibility is as low as 20 mN/m for 50% area change and steeply increases to 100 mN/m for  $\sim 100\%$  expansion, exhibiting a strain stiffening behavior. Since the results are in good agreement with the AA simulations,<sup>21</sup> the

proposed CG model of peptidoglycan can be reliably used for in silico investigations of bacterial cell walls under tension as high as 30 mN/m.

**Bending Modulus.** We have also computed the bending modulus of the model membranes of peptidoglycan using the Helfrich analysis of the membrane height fluctuations.<sup>57</sup> A surface is constructed through the peptidoglycan, and its thermal fluctuations are analyzed in the Fourier domain. Referring to Figure 11B, the static structure factor corresponding to the height fluctuations of the peptidoglycan surface is computed using Fourier transforms  $S(q) \equiv \langle \tilde{h}(\mathbf{q}) \tilde{h}^*(\mathbf{q}) \rangle_{A_0}$ , over the surface area  $A_0$  for a tensionless membrane.<sup>58–60</sup> The wave vector  $\mathbf{q} = 2\pi(n_x/L_x, n_y/L_y)$ , with integer numbers  $n_x$  and  $n_y$ , where the linear dimensions in two orthogonal directions are  $L_x$  and  $L_y$ . In the low  $\mathbf{q}$  limit, the structure factor for a

thermally fluctuating and tensionless two-dimensional surface follows

$$S(q) = k_B T / \kappa_c q^4 \quad (9)$$

The bending modulus ( $\kappa_c$ ) is deduced by fitting the structure factor data to eq 9. As evident in Figure 11B the structure factor follows  $q^4$  scaling and the data for the MARTINI network of peptidoglycan are in excellent agreement with the structure factor obtained using the AA model. An inset in Figure 11B clearly indicates that the structure factor data obey a limiting behavior with an intercept  $k_B T / \kappa_c \sim 1$ . The low value of  $\kappa_c \sim 1 k_B T$  implies that a monolayer of peptidoglycan has a smaller bending modulus when compared with lipid membranes, which possess the bending modulus of typically tens of  $k_B T$  depending on whether the lipid membrane is in gel or liquid-crystalline phase. With  $\kappa_c \sim 1 k_B T$  and  $K_a \sim 10$  mN/m for the tensionless network of peptidoglycan, the mechanical thickness of the network can be obtained using the elastic ratio,<sup>61</sup>  $\sqrt{12\kappa_c/K_a} = 2.3$  nm. This is in good agreement with the thickness of the monolayer of the peptidoglycan discussed in the preceding section.

**Potential of Mean Force Calculations.** In order to study interactions of the model peptidoglycan with small molecules, we evaluated the potential of mean force (PMF) between a thymol molecule and the peptidoglycan networks described earlier. Prior to quantifying the free energy landscapes by umbrella sampling simulations, we carried out restraint-free simulations. Figures 12A,B depict a sample translocation event observed in AA and MARTINI restraint-free simulations, respectively. The translocation of thymol through peptidoglycan occurs rapidly over a time scale of 2 ns, indicating that peptidoglycan does not offer any significant barrier for thymol.

Figure 13 illustrates the free energy of translocation for thymol across peptidoglycan. The densities of glycan, peptides,

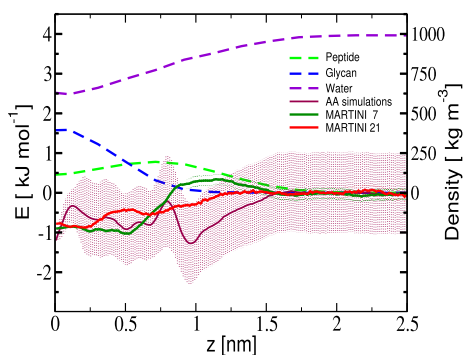


**Figure 13.** Potential of mean force for thymol interacting with peptidoglycan networks along the reaction coordinate  $z$ . The MARTINI profiles for PG network-1 (green) and PG network-2 (red) seem to accurately capture the free energy difference obtained in the all-atom simulations (maroon). The dashed lines indicate density profiles for sugar strands (blue), peptides (green) and water (violet).

and water are also indicated in Figure 13 to provide an appropriate spatial reference. The free energy profiles clearly indicate the absence of any significant barrier for thymol and the observed differences in free energies across the models lie within  $\sim 1.5$  kJ/mol with the greatest differences located at  $\sim 1$  nm in the vicinity of the peptide residues. We note that the variations in the free energy is less than  $RT$  (where  $R$  is the gas

constant) at room temperature indicating the absence of any significant barrier for thymol translocation across peptidoglycan. The all-atom free energy profile was obtained by carrying out simulations for 150 ns at each window during umbrella sampling. In order to ascertain if these sampling times were sufficient, we evaluated the variation in the PMF from a 100 ns sampling to 150 ns in steps of 10 ns. The free energy profiles had similar spatial variations, and the differences were within 0.5 kJ/mol indicating that the sampling time of 150 ns was sufficient (Figure S16 in the SI). Since the barriers in the PMFs are less than  $RT$  at room temperature, free passage of thymol is expected to occur through peptidoglycan as illustrated in the restraint-free simulations. Hence longer sampling times, which are typically required for free energy computations involving large barriers, are not required. In order to further assess the role of kinetic barriers, we analyzed the diffusion coefficients for thymol using position autocorrelation functions.<sup>62</sup> The diffusion coefficients ( $D$ ) were found to be in a range  $5\text{--}10 \times 10^{-10} \text{ m}^2 \text{ s}^{-1}$ . Given that the thickness ( $L$ ) of the peptidoglycan is about 4 nm, the corresponding diffusion time ( $L^2/D$ ) ranges from about 15–40 ns which is well within our sampling times used in the umbrella sampling.

For the MARTINI models we contrast the free energy of translocation for the smaller tethered PG network-1, with the larger PG network-2 where both the glycan strands as well as the peptides are covalently bonded with their nearest periodic images. The PG network-2 in the AA description, which contains nearly half a million interacting sites, is computationally intractable for PMF calculations by umbrella samplings and hence we did not pursue this here. Although there are differences between the two PMFs obtained for the two MARTINI models, these lie with 0.7 kJ/mol and the corresponding errors bars of  $\sim 0.12$  kJ/mol lie well within the thermal energy scale at room temperature. Although, at these low insertion free energies, these differences do not have any consequence for thymol translocation, the free energy profile with PG network-2 captures the average trends in the AA free energy profile more realistically. To conclude this section, the observation of frequent translocation of thymol in the restraint-free simulations, together with the free energy profiles, indicate that thymol can easily traverse through peptidoglycan at room temperature, in contrast to its permeation through the inner and outer bacterial membranes.<sup>63</sup>

## SUMMARY AND CONCLUSIONS

The present work proposes a MARTINI model of peptidoglycan. The model is parametrized by mapping the distributions for bonded interactions with the virtual CG distributions obtained from all-atom simulations. The issue of aggregation observed while simulating sugars and proteins<sup>36,37</sup> with the MARTINI force field is alleviated by scaling the energy parameter for nonbonded interactions. We use a uniform scaling parameter which effectively reduces the van der Waals energy,  $\epsilon$  to accurately capture the end-to-end distance of the peptidoglycan chain. As summarized in Table 8, the model parametrization is sufficient to accurately reproduce structural properties such as the native periodicity of peptide orientation, membrane thickness, cavity size distributions, and area-per-disaccharide. Additionally the response to areal expansion against lateral stresses is in good agreement with values reported in literature and the bending modulus for the model peptidoglycan is  $\sim 1 k_B T$ . In particular, the relative

orientation of peptides that are present in a 4-fold symmetry in a peptidoglycan chain is accurately captured comparing well with experimental observations further attesting to the accuracy of the scaled energy parameter. Finally the insertion free energy of thymol using the reparametrized MARTINI force field was found to compare well with the all-atom simulations without resorting to additional parametrization. Thus the proposed MARTINI force field for peptidoglycan with appropriately scaled parameters captures both structural and mechanical properties obtained in all-atom simulations and experiments.

We point out that to alleviate the problem of strong protein–protein interactions involved in dimerization of transmembrane  $\alpha$  helices the protein–protein interactions in the MARTINI force field have to be modulated.<sup>37</sup> In contrast a single glycan strand is a combination of peptides and sugars representing a polyelectrolyte chain without the presence of any secondary structure in the protein. Thus properties such as the end-to-end distance are more appropriate while reconciling the force field for such systems. Further, the membrane is in the topology of a sheet which further alleviates the problem of aggregation encountered while studying membrane mediated protein dimerization<sup>37</sup> or aggregation of sugars<sup>36</sup> in bulk solution. However, given this inherent issue with the MARTINI parameters, the interaction and translocation of proteins through our proposed model for peptidoglycan will require additional testing. For the translocation of small organic molecules such as thymol, a commonly used antibacterial agent, we expect our parametrization to be reliable.

In summary we have successfully developed a MARTINI model for peptidoglycan which can be used to reliably assess the structural, mechanical properties as well as the insertion free energies for small molecules. It would be interesting to develop a multilayered model for peptidoglycan using the MARTINI parameters developed here and assess the changes to mechanical properties as well as insertion free energies. We expect our model to have a direct bearing on understanding the barrier properties for the peptidoglycan in Gram-negative bacteria. Furthermore, the proposed CG model will be useful in simulating phenomena associated with bacterial cell walls at larger length and time scales, overcoming the limitations of AA models.

## ■ ASSOCIATED CONTENT

### SI Supporting Information

The Supporting Information is available free of charge at <https://pubs.acs.org/doi/10.1021/acs.jctc.0c00539>.

List of itp files including force field for nonbonded interactions, a simulation movie for thymol permeation, CG mapping scheme for thymol, histograms for umbrella sampling biasing potential, simulation snapshots for glycan strand at varying scaling factors, parametric optimization algorithm, figures for bonded distributions for 16-mer glycan strands, simulation snapshots for peptidoglycan network under stressed conditions, cavity size analysis, and convergence for PMF (ZIP)

## ■ AUTHOR INFORMATION

### Corresponding Author

**K. Ganapathy Ayappa** – Department of Chemical Engineering and Centre for BioSystems Science and Engineering, Indian Institute of Science, Bangalore 560012, India; [orcid.org/0000-0001-7599-794X](https://orcid.org/0000-0001-7599-794X); Email: [ayappa@iisc.ac.in](mailto:ayappa@iisc.ac.in); Fax: +91-80-2360-8121

### Authors

**Rakesh Vaiwala** – Department of Chemical Engineering, Indian Institute of Science, Bangalore 560012, India; [orcid.org/0000-0003-1862-8659](https://orcid.org/0000-0003-1862-8659)

**Pradyumn Sharma** – Department of Chemical Engineering, Indian Institute of Science, Bangalore 560012, India

**Mrinalini Puranik** – Unilever Research & Development, Bangalore 560066, India

Complete contact information is available at: <https://pubs.acs.org/10.1021/acs.jctc.0c00539>

### Notes

The authors declare no competing financial interest.

## ■ ACKNOWLEDGMENTS

We acknowledge Unilever Research and Development (Bengaluru, India) for a research grant. We also thank the Supercomputer Education and Research Center (SERC) and Thematic Unit of Excellence on Computational Materials Science (TUE-CMS), a Department of Science and Technology (DST) supported facility at the Indian Institute of Science Bangalore. We also thank Durba Sengupta for initial discussions on the MARTINI model.

## ■ REFERENCES

- (1) Gumbart, J. C.; Beeby, M.; Jensen, G. J.; Roux, B. Escherichia coli peptidoglycan structure and mechanics as predicted by atomic-scale simulations. *PLoS Comput. Biol.* **2014**, *10*, No. e1003475.
- (2) Weidel, W.; Pelzer, H. Bagshaped macromolecules—a new outlook on bacterial cell walls. *Adv. Enzymol. Relat. Areas Mol. Biol.* **1964**, *26*, 193–232.
- (3) Velkov, T.; Thompson, P. E.; Nation, R. L.; Li, J. Structure-activity relationships of polymyxin antibiotics. *J. Med. Chem.* **2010**, *53*, 1898–1916.
- (4) Kahne, D.; Leimkuhler, C.; Lu, W.; Walsh, C. Glycopeptide and lipoglycopeptide antibiotics. *Chem. Rev.* **2005**, *105*, 425–448.
- (5) Pastagia, M.; Schuch, R.; Fischetti, V. A.; Huang, D. B. Lysins: the arrival of pathogen-directed anti-infectives. *J. Med. Microbiol.* **2013**, *62*, 1506–1516.
- (6) Vollmer, W.; Blanot, D.; De Pedro, M. A. Peptidoglycan structure and architecture. *FEMS Microbiol. Rev.* **2008**, *32*, 149–167.
- (7) Barreteau, H.; Kovač, A.; Boniface, A.; Sova, M.; Gobec, S.; Blanot, D. Cytoplasmic steps of peptidoglycan biosynthesis. *FEMS Microbiol. Rev.* **2008**, *32*, 168–207.
- (8) Yao, X.; Jericho, M.; Pink, D.; Beveridge, T. Thickness and elasticity of gram-negative murein sacculi measured by atomic force microscopy. *J. Bacteriol.* **1999**, *181*, 6865–6875.
- (9) Labischinski, H.; Goodell, E.; Goodell, A.; Hochberg, M. Direct proof of a “more-than-single-layered” peptidoglycan architecture of Escherichia coli W7: a neutron small-angle scattering study. *J. Bacteriol.* **1991**, *173*, 751–756.
- (10) Gan, L.; Chen, S.; Jensen, G. J. Molecular organization of Gram-negative peptidoglycan. *Proc. Natl. Acad. Sci. U. S. A.* **2008**, *105*, 18953–18957.
- (11) Glauner, B.; Höltje, J.; Schwarz, U. The composition of the murein of Escherichia coli. *J. Biol. Chem.* **1988**, *263*, 10088–10095.

- (12) Harz, H.; Burgdorf, K.; Höltje, J.-V. Isolation and separation of the glycan strands from murein of *Escherichia coli* by reversed-phase high-performance liquid chromatography. *Anal. Biochem.* **1990**, *190*, 120–128.
- (13) Braun, V.; Gnirke, H.; Henning, U.; Rehn, K. Model for the structure of the shape-maintaining layer of the *Escherichia coli* cell envelope. *J. Bacteriol.* **1973**, *114*, 1264–1270.
- (14) Höltje, J.-V. Growth of the stress-bearing and shape-maintaining murein sacculus of *Escherichia coli*. *Microbiol. Mol. Biol. Rev.* **1998**, *62*, 181–203.
- (15) Dmitriev, B.; Toukach, F.; Ehlers, S. Towards a comprehensive view of the bacterial cell wall. *Trends Microbiol.* **2005**, *13*, 569–574.
- (16) Huang, K. C.; Mukhopadhyay, R.; Wen, B.; Gitai, Z.; Wingreen, N. S. Cell shape and cell-wall organization in Gram-negative bacteria. *Proc. Natl. Acad. Sci. U. S. A.* **2008**, *105*, 19282–19287.
- (17) Nguyen, L. T.; Gumbart, J. C.; Beeby, M.; Jensen, G. J. Coarse-grained simulations of bacterial cell wall growth reveal that local coordination alone can be sufficient to maintain rod shape. *Proc. Natl. Acad. Sci. U. S. A.* **2015**, *112*, E3689–E3698.
- (18) Leps, B.; Labischinski, H.; Bradaczek, H. Conformational behavior of the polysaccharide backbone of murein. *Biopolymers* **1987**, *26*, 1391–1406.
- (19) Koch, A. L. Simulation of the conformation of the murein fabric: the oligoglycan, penta-muropeptide, and cross-linked nona-muropeptide. *Arch. Microbiol.* **2000**, *174*, 429–439.
- (20) Meroueh, S. O.; Bencze, K. Z.; Heseck, D.; Lee, M.; Fisher, J. F.; Stemmler, T. L.; Mobashery, S. Three-dimensional structure of the bacterial cell wall peptidoglycan. *Proc. Natl. Acad. Sci. U. S. A.* **2006**, *103*, 4404–4409.
- (21) Hwang, H.; Paracini, N.; Parks, J. M.; Lakey, J. H.; Gumbart, J. C. Distribution of mechanical stress in the *Escherichia coli* cell envelope. *Biochim. Biophys. Acta, Biomembr.* **2018**, *1860*, 2566–2575.
- (22) Pushkaran, A. C.; Nataraj, N.; Nair, N.; Götz, F.; Biswas, R.; Mohan, C. G. Understanding the structure–function relationship of lysozyme resistance in *Staphylococcus aureus* by peptidoglycan O-acetylation using molecular docking, dynamics, and lysis assay. *J. Chem. Inf. Model.* **2015**, *55*, 760–770.
- (23) Kim, S.; Pires, M. M.; Im, W. Insight into elongation stages of peptidoglycan processing in bacterial cytoplasmic membranes. *Sci. Rep.* **2018**, *8*, 17704.
- (24) Piggot, T. J.; Holdbrook, D. A.; Khalid, S. Electroporation of the *E. coli* and *S. aureus* membranes: molecular dynamics simulations of complex bacterial membranes. *J. Phys. Chem. B* **2011**, *115*, 13381–13388.
- (25) Piggot, T. J.; Holdbrook, D. A.; Khalid, S. Conformational dynamics and membrane interactions of the *E. coli* outer membrane protein FecA: a molecular dynamics simulation study. *Biochim. Biophys. Acta, Biomembr.* **2013**, *1828*, 284–293.
- (26) Hsu, P.-C.; Jefferies, D.; Khalid, S. Molecular dynamics simulations predict the pathways via which pristine fullerenes penetrate bacterial membranes. *J. Phys. Chem. B* **2016**, *120*, 11170–11179.
- (27) Samsudin, F.; Boags, A.; Piggot, T. J.; Khalid, S. Braun's lipoprotein facilitates OmpA interaction with the *Escherichia coli* cell wall. *Biophys. J.* **2017**, *113*, 1496–1504.
- (28) Boags, A. T.; Samsudin, F.; Khalid, S. Binding From both sides: TolR and full-length OmpA bind and maintain the local structure of the *E. coli* cell wall. *Structure* **2019**, *27*, 713–724.
- (29) Marrink, S. J.; Risselada, H. J.; Yefimov, S.; Tieleman, D. P.; De Vries, A. H. The MARTINI force field: coarse grained model for biomolecular simulations. *J. Phys. Chem. B* **2007**, *111*, 7812–7824.
- (30) López, C. A.; Rzepiela, A. J.; De Vries, A. H.; Dijkhuizen, L.; Hünenberger, P. H.; Marrink, S. J. MARTINI coarse-grained force field: extension to carbohydrates. *J. Chem. Theory Comput.* **2009**, *5*, 3195–3210.
- (31) Monticelli, L.; Kandasamy, S. K.; Periole, X.; Larson, R. G.; Tieleman, D. P.; Marrink, S.-J. The MARTINI coarse-grained force field: extension to proteins. *J. Chem. Theory Comput.* **2008**, *4*, 819–834.
- (32) Uusitalo, J. J.; Ingólfsson, H. I.; Akhshi, P.; Tieleman, D. P.; Marrink, S. J. MARTINI coarse-grained force field: extension to DNA. *J. Chem. Theory Comput.* **2015**, *11*, 3932–3945.
- (33) Uusitalo, J. J.; Ingólfsson, H. I.; Marrink, S. J.; Faustino, I. MARTINI coarse-grained force field: extension to RNA. *Biophys. J.* **2017**, *113*, 246–256.
- (34) López, C. A.; Sovova, Z.; van Eerden, F. J.; de Vries, A. H.; Marrink, S. J. MARTINI force field parameters for glycolipids. *J. Chem. Theory Comput.* **2013**, *9*, 1694–1708.
- (35) Marrink, S. J.; Tieleman, D. P. Perspective on the MARTINI model. *Chem. Soc. Rev.* **2013**, *42*, 6801–6822.
- (36) Schmalhorst, P. S.; Deluweit, F.; Scherrers, R.; Heisenberg, C.-P.; Sikora, M. Overcoming the limitations of the MARTINI force field in simulations of polysaccharides. *J. Chem. Theory Comput.* **2017**, *13*, 5039–5053.
- (37) Javanainen, M.; Martinez-Seara, H.; Vattulainen, I. Excessive aggregation of membrane proteins in the MARTINI model. *PLoS One* **2017**, *12*, No. e0187936.
- (38) Stark, A. C.; Andrews, C. T.; Elcock, A. H. Toward optimized potential functions for protein–protein interactions in aqueous solutions: osmotic second virial coefficient calculations using the MARTINI coarse-grained force field. *J. Chem. Theory Comput.* **2013**, *9*, 4176–4185.
- (39) Carpenter, T. S.; Parkin, J.; Khalid, S. The free energy of small solute permeation through the *Escherichia coli* outer membrane has a distinctly asymmetric profile. *J. Phys. Chem. Lett.* **2016**, *7*, 3446–3451.
- (40) Ferreira, R. J.; Kasson, P. M. Antibiotic uptake across Gram-negative outer membranes: Better predictions towards better antibiotics. *ACS Infect. Dis.* **2019**, *5*, 2096–2104.
- (41) Guo, J.; Chia, G. W.; Berezhnoy, N. V.; Cazenave-Gassiot, A.; Kjelleberg, S.; Hinks, J.; Mu, Y.; Seviour, T. Bacterial lipopolysaccharide core structures mediate effects of butanol ingress. *Biochim. Biophys. Acta, Biomembr.* **2020**, *1862*, 183150.
- (42) Berendsen, H. J.; van der Spoel, D.; van Drunen, R. GROMACS: a message-passing parallel molecular dynamics implementation. *Comput. Phys. Commun.* **1995**, *91*, 43–56.
- (43) Nosé, S. A molecular dynamics method for simulations in the canonical ensemble. *Mol. Phys.* **1984**, *52*, 255–268.
- (44) Hoover, W. G. Canonical dynamics: Equilibrium phase-space distributions. *Phys. Rev. A: At., Mol., Opt. Phys.* **1985**, *31*, 1695–1697.
- (45) Parrinello, M.; Rahman, A. Polymorphic transitions in single crystals: A new molecular dynamics method. *J. Appl. Phys.* **1981**, *52*, 7182–7190.
- (46) Darden, T.; York, D.; Pedersen, L. Particle mesh Ewald: An Nlog(N) method for Ewald sums in large systems. *J. Chem. Phys.* **1993**, *98*, 10089–10092.
- (47) Bussi, G.; Donadio, D.; Parrinello, M. Canonical sampling through velocity rescaling. *J. Chem. Phys.* **2007**, *126*, 014101.
- (48) Tironi, I. G.; Sperb, R.; Smith, P. E.; van Gunsteren, W. F. A generalized reaction field method for molecular dynamics simulations. *J. Chem. Phys.* **1995**, *102*, 5451–5459.
- (49) Vanommeslaeghe, K.; Hatcher, E.; Acharya, C.; Kundu, S.; Zhong, S.; Shim, J.; Darian, E.; Guvench, O.; Lopes, P.; Vorobyov, I.; Mackerell, A. D. CHARMM general force field: A force field for drug-like molecules compatible with the CHARMM all-atom additive biological force fields. *J. Comput. Chem.* **2009**, *31*, 671–690.
- (50) Berau, T.; Kremer, K. Automated parametrization of the coarse-grained MARTINI force field for small organic molecules. *J. Chem. Theory Comput.* **2015**, *11*, 2783–2791.
- (51) Torrie, G. M.; Valleau, J. P. Nonphysical sampling distributions in Monte Carlo free-energy estimation: Umbrella sampling. *J. Comput. Phys.* **1977**, *23*, 187–199.
- (52) Hub, J. S.; De Groot, B. L.; Van Der Spoel, D. g\_wham- A free weighted histogram analysis implementation including robust error and autocorrelation estimates. *J. Chem. Theory Comput.* **2010**, *6*, 3713–3720.
- (53) Bulacu, M.; Goga, N.; Zhao, W.; Rossi, G.; Monticelli, L.; Periole, X.; Tieleman, D. P.; Marrink, S. J. Improved angle potentials

for coarse-grained molecular dynamics simulations. *J. Chem. Theory Comput.* **2013**, *9*, 3282–3292.

(54) Abraham, M. J.; Murtola, T.; Schulz, R.; Páll, S.; Smith, J. C.; Hess, B.; Lindahl, E. GROMACS: High performance molecular simulations through multi-level parallelism from laptops to supercomputers. *SoftwareX* **2015**, *1*, 19–25.

(55) Wientjes, F.; Woldringh, C.; Nanninga, N. Amount of peptidoglycan in cell walls of gram-negative bacteria. *J. Bacteriol.* **1991**, *173*, 7684–7691.

(56) Walton, J.; Tildesley, D.; Rowlinson, J.; Henderson, J. The pressure tensor at the planar surface of a liquid. *Mol. Phys.* **1983**, *48*, 1357–1368.

(57) Helfrich, W. Steric interaction of fluid membranes in multilayer systems. *Z. Naturforsch., A: Phys. Sci.* **1978**, *33*, 305–315.

(58) Thakkar, F. M.; Maiti, P. K.; Kumaran, V.; Ayappa, K. Verifying scalings for bending rigidity of bilayer membranes using mesoscale models. *Soft Matter* **2011**, *7*, 3963–3966.

(59) Brandt, E. G.; Braun, A. R.; Sachs, J. N.; Nagle, J. F.; Edholm, O. Interpretation of fluctuation spectra in lipid bilayer simulations. *Biophys. J.* **2011**, *100*, 2104–2111.

(60) Vaiwala, R.; Thaokar, R. Probing entropic repulsion through mesoscopic simulations. *EPL* **2017**, *120*, 48001.

(61) Boal, D. *Mechanics of the Cell*; Cambridge University Press, 2012.

(62) Hummer, G. Position-dependent diffusion coefficients and free energies from Bayesian analysis of equilibrium and replica molecular dynamics simulations. *New J. Phys.* **2005**, *7*, 34.

(63) Sharma, P.; Parthasarathi, S.; Patil, N.; Waskar, M.; Raut, J. S.; Puranik, M.; Ayappa, K. G.; Basu, J. K. Assessing barriers for antimicrobial penetration in complex asymmetric bacterial membranes: A case study with thymol. *Langmuir* **2020**, DOI: [10.1021/acs.langmuir.0c01124](https://doi.org/10.1021/acs.langmuir.0c01124).